EQUIVALENT PROPERTIES FOR PERFORATED PLATES - AN ANALYTICAL APPROACH

M.M. Cepkauskas*
CEP Engineering, P.O. BOX 116, Eastham, Massachusetts, 02642, U.S.A.

Jianfeng Yang
FRAMATOME-ANP Inc., Lynchburg, Virginia, U.S.A.

ABSTRACT
Structures that contain perforated plates have been a subject of interest in the Nuclear Industry. Steam generators, condensers and reactor internals utilize plates containing holes which act as flow holes or separate structures from flow by using a "tube bank" design. The equivalent plate method has been beneficial in analyzing perforate plates. Details are found in various papers found in the bibliography. In addition the ASME code addresses perforated plates in Appendix A-8000, but is limited to a triangular hole pattern. This early work performed in this field utilized test data and analytical approaches.

This paper is an examination of an analytical approach for determining equivalent plate mechanical and thermal properties. First a patch of the real plate is identified that provides a model for the necessary physical behavior of the plate. The average strain of this patch is obtained by first applying simplified one dimensional mechanical load to the patch, determining stress as a function of position, converting the stress to strain and then integrating the strain over the patch length. This average strain is then equated to the average strain of an equivalent fictitious rectangular patch. This results in obtaining equivalent Young's Modulus and Poison's Ratio for the equivalent plate in all three orthogonal directions. The corresponding equivalent shear modulus in all three directions is then determined. An orthotropic material stress strain matrix relationship is provided for the fictitious properties. By equating the real average strain with the fictitious average strain in matrix form, a stress multiplier is found to convert average fictitious stress to average real stress. This same type of process is repeated for heat conduction coefficients and coefficients of thermal expansion. Results are provided for both a square and triangular hole pattern.

Reasonable results are obtained when comparing the effective Young's Modulus and Poison's Ratio with ASME Code results. This simplified analytical approach, however, is not intended to be a precise mathematical tool for equivalent plate properties, but is used as a primer for future work in which the same approach will be used via finite element analysis.

Keywords: stress, perforated plates, ASME Code

1.0 INTRODUCTION
Various aspects of perforated plates have been the subject of publications for over a half of a century. Horvay (1951) addressed thermal stresses and later the plane stress problem for the perforated plate using an analytical approach. A great deal of literature comes from the work of O'Donnell (1962) and subsequent publications with many other authors. His work was both purely theoretical in determining ligament stresses and experimental in determining effective elastic constants using strain measurements and photo elastic testing. Theoretical values of effective elastic constants were addressed by Meijers (1967). More recent approaches to the perforated plate using Finite Element Analysis (FEA) is found in the publications by Ukadgaonker et al (1998). The list of contributors to this field is extensive. For a recent review see Ukadgaonker et al (1996).

2.0 MATHEMATICAL MODEL
Consider the one dimensional tensile loading of a plate with a triangular hole pattern as shown in Figure 1-a. Typically a tensile test would be performed with the load being quasi statically applied in increments. The resulting stress strain curve would provide the equivalent Young's Modulus E*. The measurement of the ratio of longitudinal strain versus lateral strain would produce an equivalent Poison's ration, ν^*. This new Young's Modulus and Poison's Ratio can be used in a finite element model to represent the perforated plate, but would be modeled as a solid plate. This greatly reduces computer size and gives a description of the general behavior when an in-plane force is applied.

A closer look at the plate in figure 1-a with a triangular hole pattern with pitch p, ligament dimension h and with the plate having n times F tensile load with n individual strips of width p (n was taken as 4 in the figures). The ligament efficiency is defined as η = h/p. To obtain gross behavior, it appears reasonable that one can examine one strip as shown in figure 1-b to get gross behavior of this strip. It can be further recognized that one patch of the perforated plate as shown in Figure 1-c is repeated along the strip of figure 1-b.

2.1 EQUIVALENT ELASTIC PROPERTIES

Thus an equivalent fictitious solid plate section of width p and length √3P/2 is desired to represent the behavior of the same section given in Figure 2-c. To have the overall behavior of the equivalent plate and fictitious plate to be the same the strains for the two plates must be equal.

The average strain, in the x-direction of the equivalent plate segment is:

$$\overline{\varepsilon_x^*} = F/(tP\,E_x^*) \tag{1}$$

The average real strain in the perforated plate segment would be:

$$\overline{\varepsilon_x} = \frac{1}{P\sqrt{3}/2}\int_0^{P\sqrt{3}/2}\varepsilon(x)dx \tag{2}$$

The integration of equation 2 is performed by taking the simple one dimensional stress-strain relation ship as

$\varepsilon(x) = \dfrac{\sigma(x)}{E_x}$, noting that $\sigma(x) = \dfrac{F}{Pt}$ for the region $r_0 \le x \le P\dfrac{\sqrt{3}}{2} - r_0$ & $\sigma(x) = \dfrac{F}{t(P-2y)}$ for the two regions $0 \le x \le r_0$ & $\dfrac{P\sqrt{3}}{2} - r_0 \le x \le P\dfrac{\sqrt{3}}{2}$ and recognizing that $y = \sqrt{r_0{}^2 - x^2}$ at the perimeter of the holes resulting in:

$$\overline{\varepsilon_x} = \frac{F}{PtE_x} f(\eta) \tag{3-a}$$

$$f(\eta) = \frac{4}{\sqrt{3}}\{-\frac{\pi}{6} + \frac{2}{\sqrt{\eta(2-\eta)}}Tan^{-1}[\frac{(2-\eta)Tan(\frac{\pi}{12})}{\sqrt{\eta(2-\eta)}}]\} + \frac{2\eta}{\sqrt{3}} - \frac{2\eta_{critical-x}}{\sqrt{3}} \tag{3-b}$$

This formulation is valid for ligament efficiencies from 100% to $\eta_{critical-x} = 1 - \dfrac{\sqrt{3}}{2} = 13.39\%$. The critical Efficiency occurs when the holes become large enough to start to overlap or when $r_{0critical-x} = \dfrac{1}{2}(\dfrac{P\sqrt{3}}{2})$. The integration was facilitated by several transformations consisting of $\zeta = \dfrac{x}{P}$, $\alpha = 1-\eta$ & $y = \alpha \sin\Theta$ and Integral # 446.01 & # 446.00 (Dwight 1947).

Equating equation (3-a) with equation (1) results in:

$$\frac{E_x^*}{E_x} = \frac{1}{f(\eta)} \tag{4}$$

It should be first noted that the stress is a simple one dimensional approximation. A more exact analytical approach can be considered, for example, by utilizing a two dimensional Airy's stress function. However, it needs to be emphasized that the present treatment is used mainly as a tool to understand the problem and eventually introduce the same concept using accurate stress distributions from a finite element model of the patch.

The above process when repeated for pure out of plane bending moments M_y provides identical results since the area moment of inertia for the equivalent plate is $pt^3/12$ and for the real plate is (P-2y) $t^3/12$, thus the same integration exists and $t^3/12$ terms cancel when the strains are equated.

The above process can next be repeated to find an equivalent Poisson's ratio in the y-direction due to a load in the x-direction by changing the strains to the y-direction and multiplying the right hand side of equations (1) & (2) υ_{yx}^* & υ_{yx}, respectively. This results in the simple expression: $\upsilon_{yx}^* = \upsilon_{yx}$

The above is now repeated for loading in the y-direction resulting in:

$$\frac{E_y^*}{E_y} = \frac{1}{g(\eta)} \tag{5}$$

$$g(\eta) = 2\sqrt{3}\{-\theta + \frac{2}{\sqrt{1-\frac{1}{\sqrt{3}}(1-\eta)^2}} Tan^{-1}[\frac{1+\frac{1}{\sqrt[1/4]{3}}(1-\eta)}{\sqrt{1-\frac{1}{\sqrt{3}}(1-\eta)^2}} Tan(\frac{\theta}{2})]\} + 4\eta - 4\eta_{critical-y} \tag{6}$$

This formulation is valid for ligament efficiencies from 100% to $\eta_{critical-y} = 50\%$. Poisson's Ratio is identical to that for the x-direction loading. $\theta = Sin^{-1}(1/\sqrt[1/4]{3})$.

Loading in the Z-direction results in:

$$\frac{E_z^*}{E_z} = h(\eta) \tag{7}$$

$$h(\eta) = 1 - \frac{\pi}{2\sqrt{3}}(1-\eta)^2 \tag{8}$$

This is simply a ratio of real and fictitious areas. Again Poisson's ratio is the same as above. Knowing Young's modulus and Poisson's Ratio In all three directions one can obtain G by the standard formulae $G = \frac{E}{2(1+\nu)}$. Thus we have the 9 required material constants for the orthotropic patch.

A similar formulation for a square hole pattern results in the same equations as above with the exception that:

$$f(\eta) = g(\eta) = \{-\frac{\pi}{3} + \frac{4}{\sqrt{\eta(2-\eta)}} Tan^{-1}[\frac{(2-\eta)Tan(\frac{\pi}{12})}{\sqrt{\eta(2-\eta)}}]\} + \eta \tag{9}$$

2.2 Stress Multipliers

The stress strain relationships for the general fictitious materials and real material in Compliance Form are:

$$\begin{pmatrix} \varepsilon^*_{xx} \\ \varepsilon^*_{yy} \\ \varepsilon^*_{zz} \\ \varepsilon^*_{yz} \\ \varepsilon^*_{zx} \\ \varepsilon^*_{xy} \end{pmatrix} = \begin{pmatrix} \frac{1}{E^*_x} & \frac{-\upsilon^*_{yx}}{E^*_y} & \frac{-\upsilon^*_{zx}}{E^*_z} & 0 & 0 & 0 \\ \frac{-\upsilon^*_{yx}}{E^*_y} & \frac{1}{E^*_y} & \frac{-\upsilon^*_{zy}}{E^*_z} & 0 & 0 & 0 \\ \frac{-\upsilon^*_{zx}}{E^*_z} & \frac{-\upsilon^*_{zy}}{E^*_z} & \frac{1}{E^*_z} & 0 & 0 & 0 \\ 0 & 0 & 0 & \frac{1}{2G^*_{yz}} & 0 & 0 \\ 0 & 0 & 0 & 0 & \frac{1}{2G^*_{zx}} & 0 \\ 0 & 0 & 0 & 0 & 0 & \frac{1}{2G^*_{xy}} \end{pmatrix} \begin{pmatrix} \sigma^*_{xx} \\ \sigma^*_{yy} \\ \sigma^*_{zz} \\ \sigma^*_{yz} \\ \sigma^*_{zx} \\ \sigma^*_{xy} \end{pmatrix} \tag{10}$$

$$\begin{pmatrix} \varepsilon_{xx} \\ \varepsilon_{yy} \\ \varepsilon_{zz} \\ \varepsilon_{yz} \\ \varepsilon_{zx} \\ \varepsilon_{xy} \end{pmatrix} = \begin{pmatrix} \frac{1}{E} & \frac{-\upsilon}{E} & \frac{-\upsilon}{E} & 0 & 0 & 0 \\ \frac{-\upsilon}{E} & \frac{1}{E} & \frac{-\upsilon}{E} & 0 & 0 & 0 \\ \frac{-\upsilon}{E} & \frac{-\upsilon}{E} & \frac{1}{E} & 0 & 0 & 0 \\ 0 & 0 & 0 & \frac{1}{2G} & 0 & 0 \\ 0 & 0 & 0 & 0 & \frac{1}{2G} & 0 \\ 0 & 0 & 0 & 0 & 0 & \frac{1}{2G} \end{pmatrix} \begin{pmatrix} \sigma_{xx} \\ \sigma_{yy} \\ \sigma_{zz} \\ \sigma_{yz} \\ \sigma_{zx} \\ \sigma_{xy} \end{pmatrix} \tag{11}$$

The general fictitious material in Stiffness Form is:

$$\begin{pmatrix} \sigma^*_{xx} \\ \sigma^*_{yy} \\ \sigma^*_{zz} \\ \sigma^*_{yz} \\ \sigma^*_{zx} \\ \sigma^*_{xy} \end{pmatrix} = \begin{pmatrix} \frac{1-\upsilon^*_{yz}\upsilon^*_{zy}}{E^*_y E^*_z \Delta} & \frac{\upsilon^*_{yx}+\upsilon^*_{zx}\upsilon^*_{yz}}{E^*_y E^*_z \Delta} & \frac{\upsilon^*_{zx}+\upsilon^*_{yx}\upsilon^*_{zy}}{E^*_y E^*_z \Delta} & 0 & 0 & 0 \\ \frac{\upsilon^*_{yx}+\upsilon^*_{zx}\upsilon^*_{yz}}{E^*_y E^*_z \Delta} & \frac{1-\upsilon^*_{zx}\upsilon^*_{xz}}{E^*_z E^*_x \Delta} & \frac{\upsilon^*_{zy}+\upsilon^*_{zx}\upsilon^*_{xy}}{E^*_z E^*_x \Delta} & 0 & 0 & 0 \\ \frac{\upsilon^*_{zx}+\upsilon^*_{yx}\upsilon^*_{zy}}{E^*_y E^*_z \Delta} & \frac{\upsilon^*_{zy}+\upsilon^*_{zx}\upsilon^*_{xy}}{E^*_z E^*_x \Delta} & \frac{1-\upsilon^*_{xy}\upsilon^*_{yx}}{E^*_x E^*_y \Delta} & 0 & 0 & 0 \\ 0 & 0 & 0 & 2G^*_{yz} & 0 & 0 \\ 0 & 0 & 0 & 0 & 2G^*_{zx} & 0 \\ 0 & 0 & 0 & 0 & 0 & 2G^*_{xy} \end{pmatrix} \begin{pmatrix} \varepsilon^*_{xx} \\ \varepsilon^*_{yy} \\ \varepsilon^*_{zz} \\ \varepsilon^*_{yz} \\ \varepsilon^*_{zx} \\ \varepsilon^*_{xy} \end{pmatrix} \tag{12}$$

With $\Delta = \dfrac{1-\upsilon^*_{xy}\upsilon^*_{yx}-\upsilon^*_{yz}\upsilon^*_{zy}-\upsilon^*_{zx}\upsilon^*_{xz}-2\upsilon^*_{xy}\upsilon^*_{yz}\upsilon^*_{zx}}{E^*_x E^*_y E^*_z}$

Equations 10, 11 & 12 can now be written in Matrix notation as:

$$\varepsilon^* = C^* \sigma^* \tag{13}$$

$$\varepsilon = C\ \sigma \tag{14}$$

$$\sigma^* = C^{*-1} \varepsilon^* \tag{15}$$

All through the present analysis it has been assumed that $\varepsilon = \varepsilon^*$, thus equate equation 13 with equation 14 and solve for σ:

$$\sigma = C^* C^{-1} \sigma^* = M \sigma^* \tag{16}$$

M is a 6 X 6 matrix of stress multipliers to convert average fictitious stress to average real stresses in the plate.

2.3 Thermal properties

This same simplified approach can now be applied for thermal conductivity (K) and coefficient of thermal expansion (α). Since heat conduction is proportional to the area times K, an equivalent K* can be obtained by considering the integral of the form:

$$I = \frac{1}{\sqrt{3}/2\ P} \int_0^{\sqrt{3}/2\ P} KA(x)dx \tag{17}$$

for both the fictitious plate and the real plate. Also the average displacement is obtained by considering an integral:

$$\overline{\delta} = \frac{1}{\sqrt{3}/2\ P} \int_0^{\sqrt{3}/2\ P} \alpha L(x)dx \tag{18}$$

Since A(x) = PL(x), the integration of 18 and 19 are identical, this results in the following equations for the triangular hole pattern:

$$\frac{K_x^*}{K_x} = \frac{\alpha_x^*}{\alpha_x} = 1 - \frac{\pi}{4\sqrt{3}}(1-\eta)^2 \tag{19}$$

$$\frac{K_y^*}{K_y} = \frac{\alpha_y^*}{\alpha_{yx}} = 1 - \frac{\pi}{2\sqrt{3}}(1-\eta)^2 \tag{20}$$

The corresponding values for the square plate are:

$$\frac{K^*}{K} = \frac{\alpha^*}{\alpha} = 1 - \frac{\pi}{8}(1-\eta)^2 \tag{21}$$

3.0 DISCUSSION OF RESULTS

The resulting E*/E values from equations 3-b & 4 for the triangular patch loaded in the x-direction is plotted against the ASME Code, Appendix 8000, values in figure 3. The agreement, as expected is reasonable but not precise due to the simplification of the analytical model. Again, the intent is to use this approach as a tool to introduce the

concept of modeling a patch using FEA techniques. Poisson's ratio comparison with the code is given in figure 4. Here the agreement is reasonable for ligament efficiencies from 40% to 100%. The present model does not allow the holes to deform in an oval shape. The Code data is for a thick plate (t=2P), where the present simplified approach does not consider variations due to thickness. This behavior will be more apparent in using the FEA for the patch, thus the disagreement in the low ligament efficiency range. In addition, pitch to plate thickness ratios in the FEA model will provide additional insight to the plate behavior.

The above determination for all the effective elastic constants for the triangular and square pattern is found in figures 5 & 6, respectively. It is noted that there is not a large difference in the elastic constants for the triangular pattern versus the square pattern. Also in figure 5 it is seen that there is little difference between the ratio of E*/E in the x versus y direction. Therefore the integration below ligament efficiency of 50% was not pursued.

The suggested stress multipliers, equation 16, produce average real stresses. These multipliers increase with lower ligament efficiencies. The averaging is along the length of the plate, thus these multipliers do not produce local real stresses. This deficiency will be overcome in using this approach with Finite Elements.

The thermal properties in figure 7 show different results for the triangular patch in the Y-direction. It can be seen from figure 1-C, that the average cross sectional area for heat conduction and length for thermal expansion in the X-direction is much larger than the Y-direction.

4.0 APPLICATION TO FINITE ELEMENTS

The application to the use of FEA is apparent. The triangular patch and square patch as seen in figures 1-c & 2, respectively can now be modeled by replacing the point force with a distributed load. Care must be used in avoiding local Saint- Venant effects due to loading, thus a portion of solid material may need to be added to each end of the patch. The process, as analytical described in this paper, is then repeated using FEA to obtain equivalent structural and thermal properties. This would have, in the early years of analyzing perforated plates, eliminated the need for testing of many plates. In addition, if an unorthodox hole pattern exists or a hole pattern made up of a combination of triangular and square patterns, an equivalent patch may be recognized and modeled.

This present study does not address the influence of plate thickness. This is easily considered in the FEA analysis by simply copy and pasting layers of a thin plate patch to obtain a thick plate.

In modeling an actual plate using the equivalent properties it is recommended that equivalent patch geometry be maintained in the model. Thus, a kind of sub structure/super structure approach can be followed. That is the displacement and or forces and moments from the equivalent plate patch can be superimposed on the actual FEA patch model in lieu of using the proposed stress multipliers. Here applied forces and moments would be amplified according to the ratio of p/h.

5.0 CONCLUSIONS

A simplified analytical patch approach to the perforated plate has shown reasonable results. It is more important that this approach is viewed as a tool to understand the perforated plate behavior. The application of utilizing FEA for the patch has been outlined. This will be the subject of a future paper.

6.0 REFERENCES

G. Horvay (1951), Proceedings of the First U.S. National Congress of Applied Mechanics.
G. Horvay (1952), Journal of Applied Mechanics, vol. 19, Trans. ASME, vol. 74, pp. 355-360.
G. Horvay (1952), Journal of Applied Mechanics, vol. 19, Trans. ASME, vol. 74, pp. 122-123.
W.J. O'Donnell (1962), Doctoral Thesis, University of Pittsburg.
W.J. O'Donnell & B.F Langer (1962), Journal of Engineering for Industry.
T. Slot & W.J. O'Donnell (1971), Journal of Engineering for Industry.
W.J. O'Donnell (1973), Journal of Engineering for Industry.
P. Meijers (1967), PhD Thesis, Technical University, Delft, the Netherlands.
P. Meijers (1986), 1st International Conference on Pressure Vessel Technology, Delft, the Netherlands.
V.G. Ukadgaonker & P.A. Kale (1998), Journal of Pressure Vessel Technology, Trans. ASME, vol. 120, pp 12-16.
V.G. Ukadgaonker, P.A. Kale, N.A. Agnihorti & R.S. Babu (1996), The International Journal of Pressure Vessel and Piping, vol. 67, pp. 279-297.
Herbert Bristol Dwight, "Tables of Integrals and Other Mathematical Data", Revised Edition, The Macmillan Company, New York, 1947.

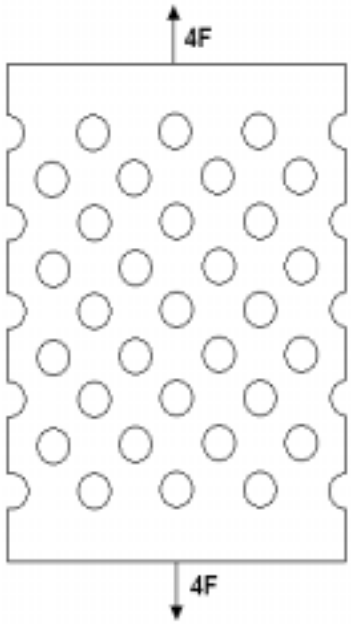

FIGURE 1-A
Tensile Test Specimen

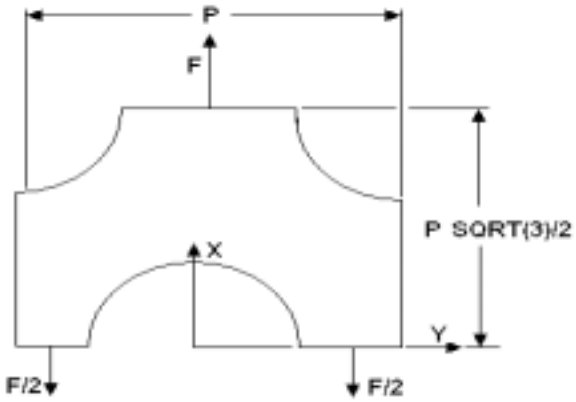

FIGURE 1-C
Triagular "Patch"

FIGURE 1-B
Typical row of Tensile Test Specimen

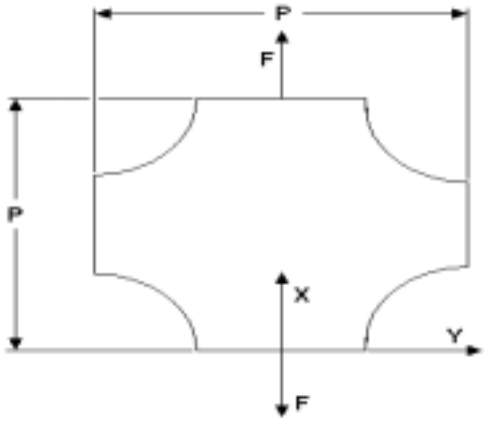

FIGURE 2
SQUARE "Patch"

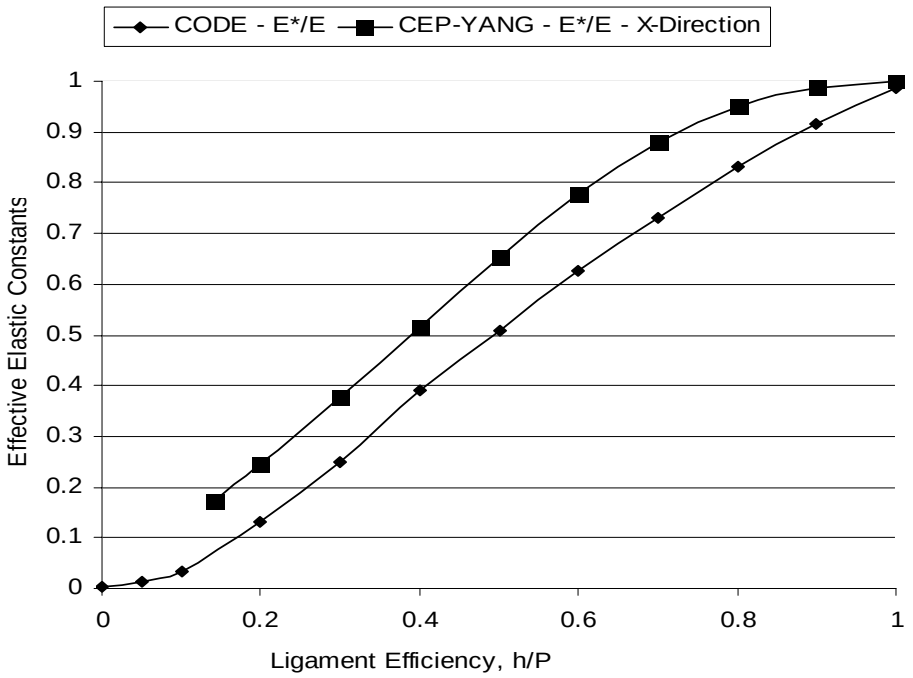

Figure 3 Modulus of Elasticity for Triangular Hole PatternComparison With ASME Code

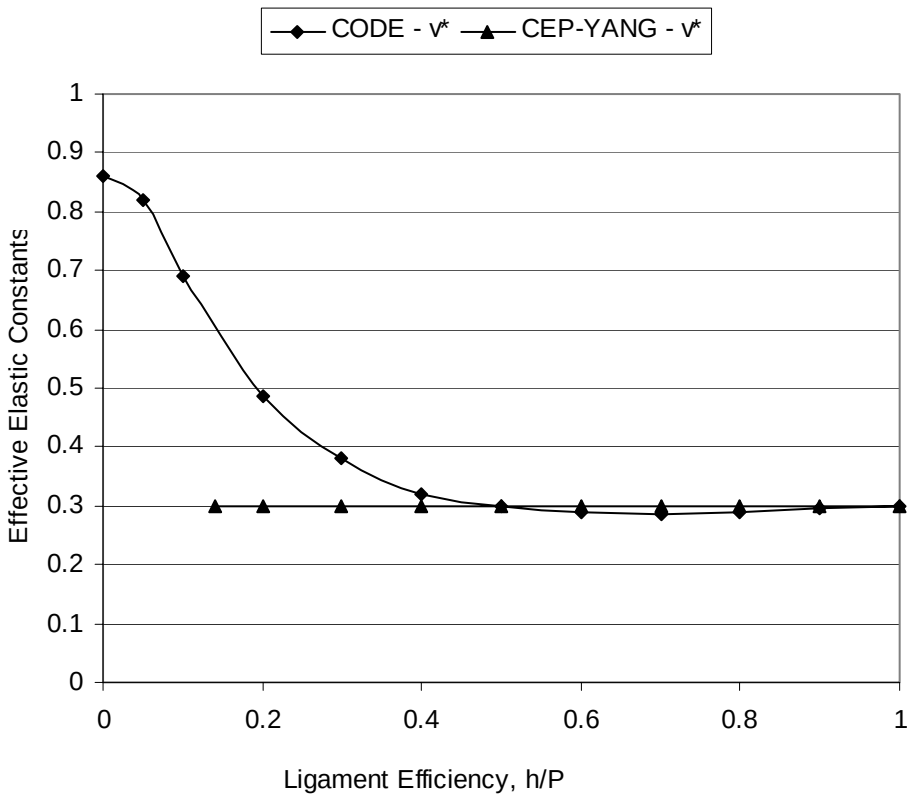

Figure 4 Poisson's Ratio Comparison With ASME Code

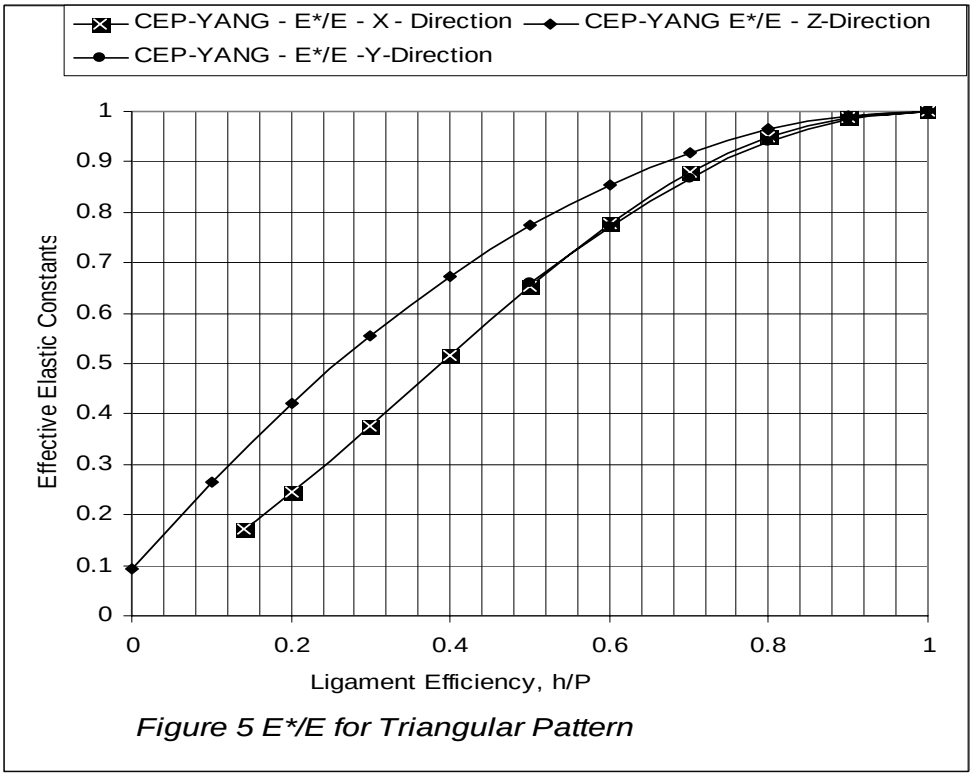

Figure 5 E/E for Triangular Pattern*

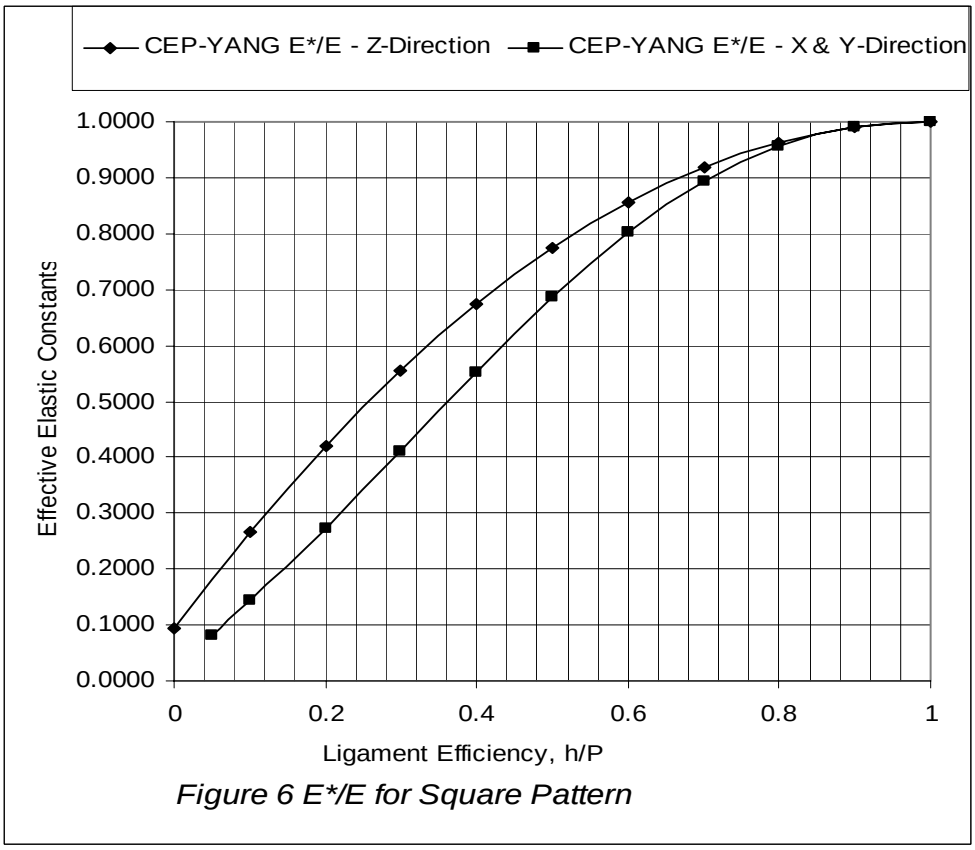

Figure 6 E/E for Square Pattern*

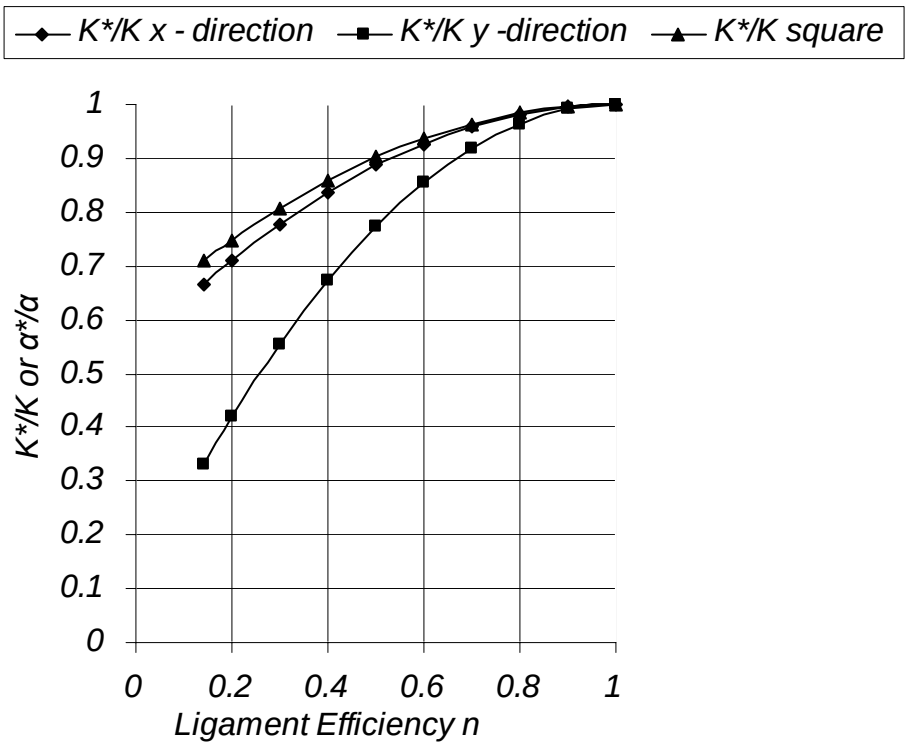

Figure 7 Thermal Properties